Metrol. Meas. Syst., Vol. 24 (2017), No. 2, pp. 289–301.

PAN POLSKA AKADEMIA NAUK

METROLOGY AND MEASUREMENT SYSTEMS

Index 330930, ISSN 0860-8229

www.metrology.pg.gda.pl

M&MS

APPLICATION OF IMPROVED ROBUST KALMAN FILTER IN DATA FUSION FOR PPP/INS TIGHTLY COUPLED POSITIONING SYSTEM

Zengke Li, Yifei Yao, Jian Wang, Jingxiang Gao

China University of Mining and Technology, School of Environment and Spatial Informatics, Xuzhou, China
(zengkeli@yeah.net, yifeiyao@163.com, wjiancumt@yeah.net, ✉ jxgaocumt@yeah.net, +86 516 8388 5785*)*

Abstract

A robust Kalman filter improved with IGG (*Institute of Geodesy and Geophysics*) scheme is proposed and used to resist the harmful effect of gross error from GPS observation in PPP/INS (*precise point positioning/inertial navigation system*) tightly coupled positioning. A new robust filter factor is constructed as a three-section function to increase the computational efficiency based on the IGG principle. The results of simulation analysis show that the robust Kalman filter with IGG scheme is able to reduce the filter iteration number and increase efficiency. The effectiveness of new robust filter is demonstrated by a real experiment. The results support our conclusion that the improved robust Kalman filter with IGG scheme used in PPP/INS tightly coupled positioning is able to remove the ill effect of gross error in GPS pseudorange observation. It clearly illustrates that the improved robust Kalman filter is very effective, and all simulated gross errors added to GPS pseudorange observation are successfully detected and modified.

Keywords: PPP/INS tightly coupled positioning, robust filter, IGG scheme, Mahalanobis distance.

© 2017 Polish Academy of Sciences. All rights reserved

1. Introduction

Integration of *Global Positioning System* (GPS) and *Inertial Navigation System* (INS) is being used more often for obtaining several high precision navigation data (position, velocity and attitude) [1]. The past integration research has been performed in different application areas (*i.e.*, monitoring, transportation, *etc.*). GPS provides highly accurate position and velocity results over extended periods in the GPS/INS integrated system, and short-term position, velocity, and attitude values are provided by INS. The GPS-alone positioning is difficult in challenging environments due to weakness and blockage of signals. INS is a self-contained velocity and attitude measurement system that does not require an external signal. Therefore, integration of GPS and INS provides enhanced performance in comparison with each individual system [2]. The *Precise Point Positioning* (PPP) using un-differenced carrier phase and pseudorange observations has been developed recently, and is capable of obtaining positions with a centimetre precision in the static mode and sub-centimetre precision in the dynamic mode. This is accomplished by using precise satellite orbits and clock correction products (*e.g.* the International GNSS Service) [3]. Some PPP and INS integration research results enable to obtain more accurate position and attitude values in the single receiver mode. With an aid of INS aid cycle slip detection and repair methods for the un-differenced GPS/MEMS (*Micro-Electromechanical Systems*) INS integrated system are proposed. These methods are capable of efficient cycle slip detection and repair, effectively increasing the positioning accuracy of the integrated system [4].

The key process between INS and other sensors in the integrated positioning system is information fusion. During the kinematic positioning, GPS signals are prone to be disturbed

Article history: received on Aug. 03, 2016; accepted on Jan. 14, 2017; available online on Jun. 30, 2017; DOI: 10.1515/mms-2017-0031.

Brought to you by | Politechnika Swietokrzyska - Kielce University of Technology
Authenticated
Download Date | 7/26/17 1:11 PM

by trees, buildings and other shelters. Thus, the performance of integrated positioning will be seriously degraded because of the gross error from GPS observation in GPS challenging environments. A robust Kalman filter could be employed to reduce the effect of gross error in GPS observation. Many forms of robust Kalman filters have been proposed in the literature. A robust Kalman filter has been researched in the last dozen or so years in different application fields, such as in-motion alignment of INS [5], SINS/SAR integrated system [6], real-time estimation of satellite clock offset [7], *precise point positioning* (PPP) [8], and others. A robust Kalman filter using the Chi square test to detect outliers in measurement was proposed in [9]. The outlier judging index was defined as the square of the Mahalanobis distance between the observed and predicted results. Based on the robust Kalman filter using the Chi square test, a robust Kalman filter improved with IGG (Institute of Geodesy and Geophysics) scheme is proposed and applied in PPP/INS tightly coupled positioning to increase its computational efficiency. The new robust filter factor is constructed as a three-section function on the basis of IGG principle.

The paper is divided into 5 sections. Following this introduction, a PPP/INS tightly coupled positioning model is overviewed in Section 2. Section 3 presents the robust Kalman filter improved with IGG scheme, and the simulation analysis corresponding to it. The field test results are then presented and analysed in Section 4, followed by a summary of the main conclusions.

2. PPP/INS tightly coupled positioning

2.1. PPP observation model

The observation models of un-differenced GPS pseudo-range, carrier phase and Doppler measurements for PPP can be expressed as follows [10]:

$$P_1 = \rho + c\cdot(dt - dt_s) + I_1 + T + M_{P_1} + \varepsilon_{P_1}, \tag{1}$$

$$P_2 = \rho + c\cdot(dt - dt_s) + \frac{f_1^2}{f_2^2} I_1 + T + M_{P_2} + \varepsilon_{P_2}, \tag{2}$$

$$\Phi_1 = \rho + c\cdot(dt - dt_s) - I_1 + T + \lambda_1 N_1 + M_{\Phi_1} + \varepsilon_{\Phi_1}, \tag{3}$$

$$\Phi_2 = \rho + c\cdot(dt - dt_s) - \frac{f_1^2}{f_2^2} I_1 + T + \lambda_2 N_2 + M_{\Phi_2} + \varepsilon_{\Phi_2}, \tag{4}$$

$$D_1 = \dot{\rho} + c\cdot(\dot{dt} - \dot{dt}_s) - \dot{I}_1 + \dot{T} + \varepsilon_{D_1}, \tag{5}$$

$$D_2 = \dot{\rho} + c\cdot(\dot{dt} - \dot{dt}_s) - \frac{f_1^2}{f_2^2} \dot{I}_1 + \dot{T} + \varepsilon_{D_2}, \tag{6}$$

where: P, Φ and D are pseudo-range, carrier phase and Doppler observations, respectively; ρ is a geometric distance between the receiver antenna and satellite phase centres; $\dot{\rho}$ is a geometric range rate; c is the velocity of light in vacuum; dt and dt_s are satellite and receiver clock errors, respectively; $\dot{dt}$ and $\dot{dt}_s$ are the satellite clock error drift and receiver clock error drift, respectively; I and $\dot{I}$ are a first-order ionospheric delay and an ionospheric delay drift, respectively; f_1 and f_2 are frequencies of the carrier phases Φ_1 and Φ_2; T and $\dot{T}$ are

Brought to you by | Politechnika Swietokrzyska - Kielce University of Technology
Authenticated
Download Date | 7/26/17 1:11 PM

a tropospheric delay and a tropospheric delay drift. Because the hydrostatic part of tropospheric delay can be predicted using models, T represents the wet component of tropospheric delay; M_P and M_Φ are multipath errors of the pseudo-range and carrier phase measurements; ε_P, ε_Φ and ε_D are combination noise values of the pseudo-range, carrier phase and Doppler measurements, and subscripts 1 and 2 refer to the observations at different frequencies.

By using the high-accuracy GPS satellite orbit and clock products, the errors in the satellite orbit and clock corrections can be significantly reduced. Other error sources including the satellite antenna phase centre offset, phase wind up, earth tide, ocean tide loading and atmosphere loading can be removed by a correction model. The widely used ionosphere-free combination makes use of the GPS radio frequency's dispersion property to mitigate the first-order ionospheric delay effect. The observation model of ionosphere-free combination can be expressed as follows [11]:

$$P_{if} = \frac{f_1^2}{f_1^2 - f_2^2} P_1 - \frac{f_2^2}{f_1^2 - f_2^2} P_2 = \rho + c \cdot (dt - dt_s) + T + M_{P_{if}} + \varepsilon_{P_{if}} , \tag{7}$$

$$\Phi_{if} = \frac{f_1^2}{f_1^2 - f_2^2} \Phi_1 - \frac{f_2^2}{f_1^2 - f_2^2} \Phi_2 = \rho + c \cdot (dt - dt_s) + T + \lambda_{if} N_{if} + M_{\Phi_{if}} + \varepsilon_{\Phi_{if}} , \tag{8}$$

$$D_{if} = \frac{f_1^2}{f_1^2 - f_2^2} D_1 - \frac{f_2^2}{f_1^2 - f_2^2} D_2 = \dot{\rho} + c \cdot (\dot{dt} - \dot{dt}_s) + \dot{T} + \varepsilon_{D_{if}} , \tag{9}$$

where a subscript *if* refers to the ionosphere-free combination observation.

Because the change of tropospheric delay is very slow, the tropospheric delay drift can be considered to be zero. The variables estimated in PPP resolution are: the three-dimensional position, receiver clock error, receiver clock error drift, zenith tropospheric delay, and ionosphere-free combination ambiguity.

2.2. Tightly coupled dynamics model

The dynamics error model of PPP/INS integrated positioning for the Kalman filter is constructed on the basis of INS error equations. The insignificant terms are neglected in the linear approximation process [12]. The error equations of INS navigation could be theoretically expressed as [13]:

$$\delta \dot{\boldsymbol{r}} = -\boldsymbol{\omega}_{\mathrm{en}} \times \delta \boldsymbol{r} + \delta \boldsymbol{v} , \tag{10}$$

$$\delta \dot{\boldsymbol{v}} = -(2\boldsymbol{\omega}_{\mathrm{ie}} + \boldsymbol{\omega}_{\mathrm{en}}) \times \delta \boldsymbol{v} - \delta \boldsymbol{\psi} \times \boldsymbol{f} + \boldsymbol{\eta} , \tag{11}$$

$$\delta \dot{\boldsymbol{\psi}} = -(\boldsymbol{\omega}_{\mathrm{ie}} + \boldsymbol{\omega}_{\mathrm{en}}) \times \delta \boldsymbol{\psi} + \boldsymbol{\varepsilon} , \tag{12}$$

where: $\delta \boldsymbol{r}$, $\delta \boldsymbol{v}$ and $\delta \boldsymbol{\psi}$ are position, velocity and orientation error vectors, respectively; $\boldsymbol{\omega}_{\mathrm{en}}$ is an angular rate of the navigation frame with respect to the earth frame, and $\boldsymbol{\omega}_{\mathrm{ie}}$ is an angular rate of the earth frame with respect to the inertial frame. The system dynamics error of PPP/INS integration navigation is obtained by expanding the accelerometer bias error vector $\boldsymbol{\eta}$ and the gyro drift error vector $\boldsymbol{\varepsilon}$.

The dynamic behaviour of accelerometer bias error $\boldsymbol{\eta}$ and gyro drift error $\boldsymbol{\varepsilon}$ usually can be modelled as a first-order Gauss-Markov process, which can be represented as follows [14]:

$$\dot{\boldsymbol{\eta}} = \frac{1}{\lambda_\eta} \boldsymbol{\eta} + \boldsymbol{u}_\eta , \tag{13}$$

Brought to you by | Politechnika Swietokrzyska - Kielce University of Technology
Authenticated
Download Date | 7/26/17 1:11 PM

$$\dot{\boldsymbol{\varepsilon}} = \frac{1}{\lambda_\varepsilon}\boldsymbol{\varepsilon} + \boldsymbol{u}_\varepsilon, \tag{14}$$

where: λ_η and λ_ε are correlation times for the accelerometers and the gyros, respectively; $\boldsymbol{u}_\eta$ and $\boldsymbol{u}_\varepsilon$ are white noise vectors of the accelerometer bias error and the gyro drift error, respectively.

The state dynamic equations of receiver clock, tropospheric delay and ionosphere-free carrier ambiguity which are related to PPP can be written as [11]:

$$\dot{dt} = \delta dt + u_{dt}, \tag{15}$$

$$\delta\dot{dt} = u_{\delta dt}, \tag{16}$$

$$\dot{T} = u_T, \tag{17}$$

$$\dot{N}_{if} = u_N, \tag{18}$$

where u_{dt}, $u_{\delta dt}$, u_T and u_N are white noise vectors of the receiver clock error, receiver clock error drift, zenith tropospheric delay and ionosphere-free carrier ambiguity, respectively.

According to the equations (10) to (18), the system dynamics model can be generalized in a matrix and vector form:

$$\dot{\boldsymbol{X}} = \boldsymbol{F}\boldsymbol{X} + \boldsymbol{u}, \tag{19}$$

wherein: $\boldsymbol{X}$ is an error state vector; $\boldsymbol{F}$ is a transition matrix and $\boldsymbol{u}$ is a process noise vector.

2.3. Tightly coupled observation model

The observation model of Kalman filter in PPP/INS integrated positioning is a vector composed of the pseudo-range, carrier phase and Doppler difference between the GPS observation and INS prediction values [15]:

$$\boldsymbol{Z} = \begin{bmatrix} P_j^{\mathrm{GPS}} - P_j^{\mathrm{INS}} \\ \Phi_j^{\mathrm{GPS}} - \Phi_j^{\mathrm{INS}} \\ D_j^{\mathrm{GPS}} - D_j^{\mathrm{INS}} \\ \vdots \end{bmatrix}, \tag{20}$$

where: P_j^{GPS}, Φ_j^{GPS} and D_j^{GPS} are ionosphere-free pseudo-range, carrier phase and Doppler values of the *j*th satellite observed by GPS, respectively; P_j^{INS}, Φ_j^{INS} and D_j^{INS} are ionosphere-free pseudo-range, carrier phase and Doppler measurement values of the *j*th satellite predicted by INS with the satellite position and velocity information, respectively.

The variable form of tightly coupled observation equation for Kalman filter can be generalized in a matrix and vector form:

$$\boldsymbol{Z}_k = \boldsymbol{H}_k\boldsymbol{X}_k + \boldsymbol{\tau}, \tag{21}$$

where: $\boldsymbol{Z}_k$ is an observation matrix; $\boldsymbol{H}_k$ is an observation equation coefficient matrix and $\boldsymbol{\tau}$ is a vector of the observation noise, assumed to be white Gaussian noise.

Brought to you by | Politechnika Swietokrzyska - Kielce University of Technology
Authenticated
Download Date | 7/26/17 1:11 PM

2.4. Tightly coupled positioning flow

Figure 1 shows a PPP/INS tightly coupled positioning system. INS mechanization is an algorithm that calculates the current position, velocity, and attitude solutions from the IMU information. Exact satellite position and clock correction information is obtained from the precise orbit and clock products. The position and velocity outputs from the INS mechanization are used to predict the pseudo-range, carrier phase, and Doppler measurements for GPS. After correcting the errors (*i.e.* satellite antenna phase centre offset, phase wind up, earth tide, ocean tide loading) in the raw GPS measurements, the difference value between the corrected pseudo-range, carrier phase, and Doppler measurement results from PPP and the INS-predicted measurement results is input into the Kalman filter as the observation vector. The final position, velocity and attitude are obtained by the filter fusion and update. Higher accuracy predictions of pseudo-range, carrier phase, and Doppler are input into the filter and compared with the traditional PPP algorithm without INS.

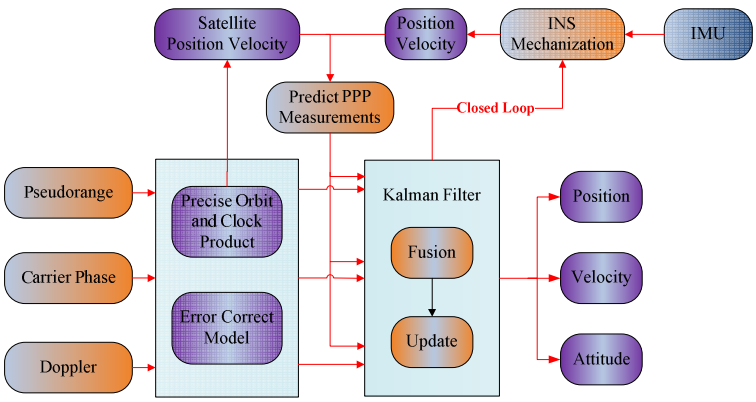

Fig. 1. A PPP/INS tightly coupled positioning system.

3. Robust Kalman filter with IGG scheme

3.1. Kalman filter

When GPS is available, the Kalman filter estimation will be employed to update the state parameters by time and observation updates in PPP/INS tightly coupled positioning. The time update process is expressed as:

$$\bar{\boldsymbol{X}}_k = \boldsymbol{F}_{k,k-1}\hat{\boldsymbol{X}}_{k-1}, \tag{22}$$

$$\bar{\boldsymbol{P}}_k = \boldsymbol{F}_{k,k-1}\boldsymbol{P}_{k-1}\boldsymbol{F}_{k,k-1}^{\mathrm{T}} + \boldsymbol{Q}_{k-1}. \tag{23}$$

The observation update equation of Kalman filter is written as:

$$\bar{\boldsymbol{V}}_k = \boldsymbol{Z}_k - \boldsymbol{H}_k\bar{\boldsymbol{X}}_k, \tag{24}$$

$$\boldsymbol{P}_{\bar{V}_k} = \boldsymbol{H}_k\bar{\boldsymbol{P}}_k\boldsymbol{H}_k^{\mathrm{T}} + \boldsymbol{R}_k, \tag{25}$$

$$\boldsymbol{G}_k = \bar{\boldsymbol{P}}_k\boldsymbol{H}_k^{\mathrm{T}}\boldsymbol{P}_{\bar{V}_k}^{-1}, \tag{26}$$

Brought to you by | Politechnika Swietokrzyska - Kielce University of Technology
Authenticated
Download Date | 7/26/17 1:11 PM

$$\hat{\boldsymbol{X}}_k = \bar{\boldsymbol{X}}_k + \boldsymbol{G}_k \bar{\boldsymbol{V}}_k, \tag{27}$$

$$\boldsymbol{P}_k = \left(\boldsymbol{I} - \boldsymbol{G}_k \boldsymbol{H}_k\right) \bar{\boldsymbol{P}}_k, \tag{28}$$

where: $\bar{\boldsymbol{X}}_k$ is an a priori state estimation; $\hat{\boldsymbol{X}}_k$ is an a posteriori state estimation; $\boldsymbol{G}_k$ is a gain matrix of Kalman filter; $\bar{\boldsymbol{P}}_k$ is an a priori covariance matrix of the state vector; $\boldsymbol{P}_k$ is an a posteriori covariance matrix of the state vector; $\boldsymbol{R}_k$ is a covariance matrix of the observation noise vector; $\boldsymbol{Q}_{k-1}$ is a covariance matrix of the process noise, a subscript k denotes a moment, and a subscript k,k-1 represents the state or covariance estimates in a period between k-1 and k moments.

In a closed loop integration scheme, a feedback loop is used for correcting the systematic errors of INS. In this way, the assumption of small errors can be employed [16]. Thus, an a posteriori state estimate is expressed as:

$$\hat{\boldsymbol{X}}_k = \bar{\boldsymbol{P}}_k \boldsymbol{H}_k^{\mathrm{T}} \left(\boldsymbol{H}_k \bar{\boldsymbol{P}}_k \boldsymbol{H}_k^{\mathrm{T}} + \boldsymbol{R}_k\right)^{-1} \boldsymbol{Z}_k. \tag{29}$$

In a closed loop, the a posteriori state estimation will be used for correcting the positioning parameters which set the a priori state estimation $\bar{\boldsymbol{X}}_k$ to zero in the next filter prediction.

3.2. Robust Kalman filter based on Mahalanobis distance

Under the Gaussian assumption, $\boldsymbol{Z}_k$ should obey a Gaussian distribution with mean $\boldsymbol{H}_k \bar{\boldsymbol{X}}$ and covariance $\boldsymbol{P}_{\bar{V}_k}$. Therefore, the squared Mahalanobis distance of $\boldsymbol{Z}_k$ should be a Chi square distribution [17], and its freedom is equal to the number of dimensions for the observation vector:

$$\gamma_k = M_k^2 = \left(\boldsymbol{Z}_k - \boldsymbol{H}_k \bar{\boldsymbol{X}}\right)^{\mathrm{T}} \left(\boldsymbol{P}_{\bar{V}_k}\right)^{-1} \left(\boldsymbol{Z}_k - \boldsymbol{H}_k \bar{\boldsymbol{X}}\right) \sim \chi_m^2, \tag{30}$$

where M_k is the Mahalanobis distance.

In order to find whether there is gross error in an observation $\boldsymbol{Z}_k$, a Chi square test is formed to determine whether the actual observation $\boldsymbol{Z}_k$ obeys a Gaussian distribution. A significant level α, the probability threshold below which the null hypothesis will be rejected, is selected. In this contribution 1% is adopted, and the corresponding upper α-quantile is $\chi_{m,\alpha}^2$:

$$\Pr\left[\gamma_k > \chi_{m,\alpha}^2\right] < \alpha, \tag{31}$$

where Pr[·] represents the probability of a random event. According to the law of Chi square distribution, the probability of γ_k being larger than $\chi_{m,\alpha}^2$ should be minute. Therefore, if the actual γ_k is larger than this α-quantile, the basic assumptions are very likely incorrect, which means that the observation is profoundly more likely disturbed by gross error.

If the index γ_k is larger than $\chi_{m,\alpha}^2$, a robust factor β is introduced to inflate the covariance matrix of measurement noise vector:

$$\bar{\boldsymbol{R}}_k = \beta_k \boldsymbol{R}_k. \tag{32}$$

The robust factor is calculated as:

$$\beta_k = \frac{\gamma_k}{\chi_{m,\alpha}^2}. \tag{33}$$

Brought to you by | Politechnika Swietokrzyska - Kielce University of Technology
Authenticated
Download Date | 7/26/17 1:11 PM

According to the above method, when γ_k is larger than $\chi^2_{m,\alpha}$, the observation $\boldsymbol{Z}_k$ is presumed to be disturbed by gross error.

3.3. Robust Kalman filter improved with IGG scheme

In the above robust Kalman filter, only one threshold value is used to identify whether the observation is with gross error or not. If the observation is disturbed by gross error, the robust factor β is calculated to implement the robust filter algorithm. In the engineering projects, the observation usually is disturbed by different levels of gross error. If the gross error is small, the observation will play a part role in the filter update by expanding the covariance matrix of measurement noise vector. If the gross error is large, the observation is of no any positive effect. In that case, the covariance matrix of measurement noise vector can be directly set to infinity to remove the negative effect of observation with gross error. So an improved robust Kalman filter is constructed by adding a new robust factor with IGG scheme to improve the calculation efficiency using a piecewise function [18]:

$$\beta_k = \begin{cases} 1 & \gamma_k \le \chi^2_{m,\alpha_0} \\ \dfrac{\gamma_k}{\chi^2_{m,\alpha}} & \chi^2_{m,\alpha_0} < \gamma_k \le \chi^2_{m,\alpha_1} \\ \infty & \chi^2_{m,\alpha_1} < \gamma_k \end{cases}. \tag{34}$$

The probabilities α_0 and α_1 are set to 1% and 0.01%, respectively. If the actual γ_k is larger than this α_1-quantile, the equivalent covariance matrix $\overline{\boldsymbol{R}}_k$ is set to ∞ rather than iteratively computed. The stage of detecting a gross error is slightly more complex and the computational efficiency is increased. Comparing the above with a plain robust Kalman filter, the main difference is in the condition when the gross error is large. An easier algorithm will be implemented and a higher efficiency will be achieved in this situation for the improved filter.

3.4. Simulation analysis

The two-dimensional kinematic positioning simulation with a constant velocity is employed. The dynamic model can be written as:

$$\begin{aligned} \dot{\boldsymbol{X}} &= \begin{bmatrix} \dot{p}_{\mathrm{N}} \\ \dot{p}_{\mathrm{E}} \\ \dot{v}_{\mathrm{N}} \\ \dot{v}_{\mathrm{E}} \end{bmatrix} = \begin{bmatrix} 0 & 0 & 1 & 0 \\ 0 & 0 & 0 & 1 \\ 0 & 0 & 0 & 0 \\ 0 & 0 & 0 & 0 \end{bmatrix} \begin{bmatrix} p_{\mathrm{N}} \\ p_{\mathrm{E}} \\ v_{\mathrm{N}} \\ v_{\mathrm{E}} \end{bmatrix} + \begin{bmatrix} 0 \\ 0 \\ \alpha_{\mathrm{N}} \\ \alpha_{\mathrm{E}} \end{bmatrix}, \\ &= \boldsymbol{\Phi X} + \boldsymbol{u} \end{aligned} \tag{35}$$

where p_{N}, p_{E}, v_{N} and v_{E} are positions and velocities in the north and east directions, respectively, α_{N} and α_{E} are the north and east accelerations, which are considered random noise in the constant velocity model. A discrete time form of the dynamical model is as follows:

$$\boldsymbol{X}_k = \boldsymbol{F}_{k,k-1}\boldsymbol{X}_{k-1} + \boldsymbol{u}_k. \tag{36}$$

The simulation test's observation data are positions in the north and east directions, so the observation model of Kalman filter is:

Brought to you by | Politechnika Swietokrzyska - Kielce University of Technology
Authenticated
Download Date | 7/26/17 1:11 PM

$$\boldsymbol{Z}_k = \boldsymbol{H}_k \boldsymbol{X}_k + \boldsymbol{\tau}_k = \begin{bmatrix} 1 & 0 & 0 & 0 \\ 0 & 1 & 0 & 0 \end{bmatrix} \begin{bmatrix} p_{\mathrm{N}} \\ p_{\mathrm{E}} \\ v_{\mathrm{N}} \\ v_{\mathrm{E}} \end{bmatrix} + \begin{bmatrix} \tau_{\mathrm{N}} \\ \tau_{\mathrm{E}} \end{bmatrix}. \tag{37}$$

The process noise $\boldsymbol{u}$ and observation noise $\boldsymbol{\tau}$ obey a Gaussian distribution. The standard deviations of process noise and observation noise are set to 0.15 m/s^2 and 1 m, respectively. The gross error case is studied to compare the performance of different construction methods of the robust factor. In the gross error case, gross errors with values of 5 m, 8 m and 20 m are added into the position observations in the north and east directions every 100 s, 200 s and 300 s, respectively, and a standard Kalman filter (scheme 1), a robust Kalman filter (scheme 2) and a robust Kalman filter with IGG scheme (scheme 3) are employed.

Figure 2 shows the values of judgment statistic γ_k. The red and green lines represent the threshold values (9.2 and 18.4) of significance levels α_0 and α_1, respectively. There are 28 values of γ_k which are less than 18.4 and greater than 9.2 and 28 values of γ_k which are greater than 18.4. Different strategies using the IGG scheme are employed to process the various levels of gross error. The position error series for different schemes is plotted in Fig. 3. The RMSs of position errors for three schemes are illustrated in Table 2. The position error for a standard Kalman filter is large due to the fact that gross errors with values of 5 m, 8 m, and 20 m are added to the position observation. As expected, both scheme 2 and scheme 3 show a very similar robust performance. The position error of scheme 2 is somewhat larger than the position error of scheme 3, which demonstrates that the robust Kalman filter with IGG principle achieves a better performance. Fig. 4 shows the filter iteration numbers for schemes 2 and 3 when gross error occurs. The sum total of filter iteration numbers for scheme 2 is greater than that for scheme 3. The filter iteration numbers of schemes 2 and 3 for the situation with gross error are 1391 and 983, respectively. Scheme 3 achieves nearly the same performance as scheme 2 and even a slightly better efficiency than scheme 2. In conclusion, scheme 3 achieves a better performance and a higher efficiency than scheme 2.

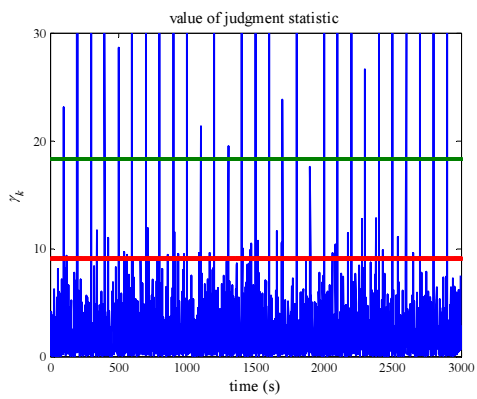

Fig. 2. The value of judgement statistic for gross error.

Brought to you by | Politechnika Swietokrzyska - Kielce University of Technology
Authenticated
Download Date | 7/26/17 1:11 PM

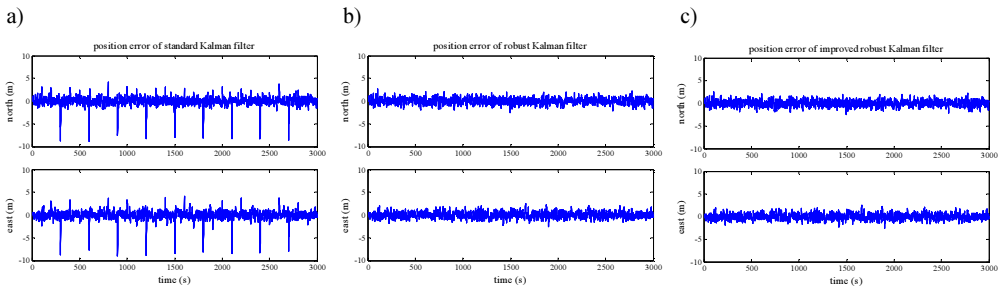

Fig. 3. Position errors for different schemes without gross error:
a standard Kalman filter (a); a robust Kalman filter (b); an improved robust Kalman filter (c).

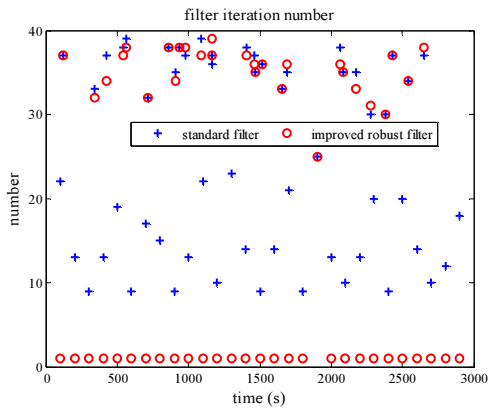

Fig. 4. The filter iteration numbers for different schemes with gross error.

Table 1. Comparison of RMSs for different schemes regarding a position error.

Scheme	North (m)	East (m)
Standard filter	0.955	0.968
Robust filter	0.654	0.653
Improved robust filter	0.651	0.649

4. Field test and analysis

A field test with one MEMS grade IMU (*Inertial Measurement Unit*), one tactical grade IMU, and two GPS receivers was performed on the roof of the *Nottingham Geospatial Institute* (NGI), and its intent was to validate performance of the proposed filter method. Initially, one Leica AS10 GNSS dual-frequency antenna was installed on the top of a pillar above the NGI locomotive. The MEMS IMU, connected to the Leica antenna, recorded raw observations onto an SD card for post-processing from inside the locomotive. The reference station consisted of another GPS receiver placed on one of the NGI roof pillars. Sampling rates of GPS receivers and IMU were set to 10 Hz and 200 Hz, respectively. The sky plots (azimuth vs. elevation) of GPS at the moving station are shown in Fig. 5. Observations from PRN3, PRN7, PRN8, PRN16, PRN18, PRN19, PRN21, PRN22 and PRN27 during the field test were available.

Brought to you by | Politechnika Swietokrzyska - Kielce University of Technology
Authenticated
Download Date | 7/26/17 1:11 PM

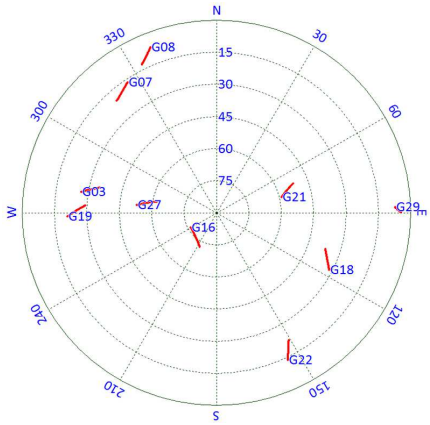

Fig. 5. Sky plots (azimuth vs. elevation) of GPS at the moving station.

The entire test was completed in approximately 20 minutes. The GPS software, GrafNav™ 8.0, was used to process GPS observation in the DGPS mode, and the solution was regarded as the position and velocity reference. The Inertial Explorer processing software generated the attitude reference using observations from two GPS receivers and one tactical grade IMU. The *root mean square* (RMS) error is used based on the reference value to obtain accuracy of different schemes. Fig. 6 presents the experience trajectory and the devices used during the test. Table 2 provides specifications of the MEMS-IMU.

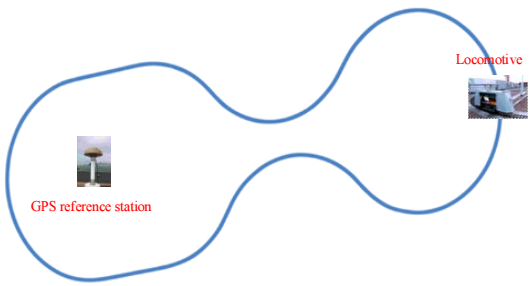

Fig. 6. A field test.

Table 2. The MEMS grade IMU technical data.

Parameters	Gyroscope	Accelerometer
Initial bias error	±0.25°/sec	±0.002 g
In-run bias stability	18°/hr	±0.04 mg
Scale factor stability	±0.05%	±0.05%
Random walk	0.03°/s/sqrt (Hz)	80 μg/sqrt (Hz)

In order to test performance of a robust Kalman filter in PPP/INS tightly positioning, the gross error case is studied, and a standard Kalman filter (scheme 1), a robust Kalman filter (scheme 2) and an improved robust Kalman filter (scheme 3) are employed. Gross errors with values of −20 m, −15 m, and 20 m were added to the pseudo-range observation on PRN7, PRN18, and PRN22 every 100 s, respectively. Gross errors with values of 10 m, −5 m, and 15 m were added to the pseudo-range observation on PRN3, PRN21, and PRN27 every 80 s, respectively.

Brought to you by | Politechnika Swietokrzyska - Kielce University of Technology
Authenticated
Download Date | 7/26/17 1:11 PM

In Fig. 7 field test trajectories for different schemes are compared. Fig. 8 shows the time series of position errors in the north, east and down directions for scheme 1, scheme 2 and scheme 3. The RMSs of position errors of three schemes are presented in Table 3. Fig. 9 shows a histogram of position errors' RMSs in the north, east and down directions for schemes 1, 2 and 3. The positioning resolution trajectory by the standard Kalman filter seriously deviates from the reference. Similarly to the simulation analysis results, accuracies of schemes 2 and 3 are again almost of the same quality. So the field test trajectories and position error curves from schemes 2 and 3 almost coincide. Scheme 3 achieves nearly the same performance as scheme 2 and even a slightly better efficiency than scheme 2 from the statistical result of RMS, which is also similar to the simulation test results. The improved robust Kalman filter is able to remove the ill effect of gross error. The RMSs of position errors in the north, east and down direction are 0.695 m, 0.875 m and 0.548 m, respectively, when the standard Kalman filter is used. However, the RMSs of position errors are 0.465 m, 0.524 m and 0.293 m, respectively, when the improved robust Kalman filter is applied. In comparison with scheme 1, the improvements are about 33%, 40% and 47% for using scheme 3 in the north, east and down directions, respectively. The position RMS of scheme 3 is 0.759 m which is better than that of scheme 1 with an improvement of 39% in the three-dimensional component. It clearly illustrates that the robust Kalman filter with IGG scheme is very effective, and all gross errors are successfully identified. Significantly, there are obvious improvements for PPP/INS tightly coupled positioning if a robust Kalman filter with IGG scheme is used. IGG scheme can be used as a very efficient filtering tool.

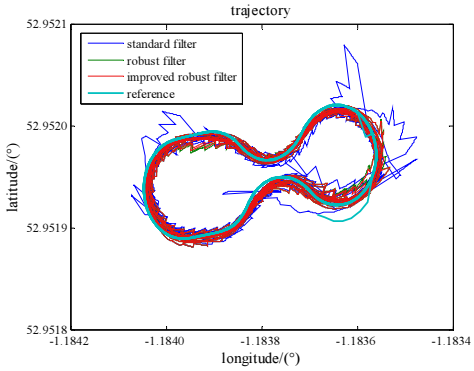

Fig. 7. Field test trajectories for different schemes with gross error.

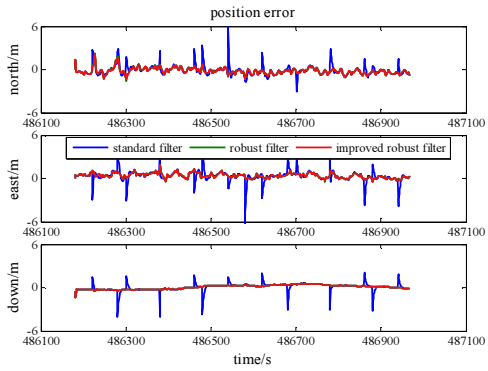

Fig. 8. Position error series for different schemes with gross error.

Brought to you by | Politechnika Swietokrzyska - Kielce University of Technology
Authenticated
Download Date | 7/26/17 1:11 PM

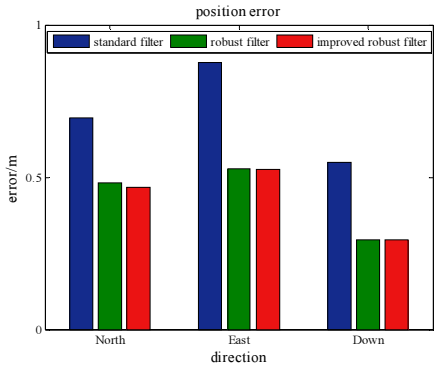

Fig. 9. Comparison of position errors for different schemes with gross error.

Table 3. Comparison of RMSs for different schemes regarding a position error.

Scheme	North (m)	East (m)	Down (m)
Standard filter	0.695	0.875	0.548
Robust filter	0.481	0.527	0.293
Improved robust filter	0.465	0.524	0.293

5. Conclusions

During the robust filter process, iterative computations will take much time, thus reducing the computational efficiency. To increase it, an improved robust scheme is proposed based on the robust Kalman filter with Mahalanobis distance and a new robust filter factor is constructed as a three-section function using the IGG principle. By simulation and comparing errors obtained for a standard Kalman filter, a robust Kalman filter based on Mahalanobis distance and an improved robust Kalman filter with the IGG principle, the improved robust Kalman filter provides the best performance and fewer filter iteration numbers than the robust Kalman filter based on Mahalanobis distance.

A PPP/INS tightly coupled positioning experiment was carried out to further validate the performance of the proposed filtering method. The position accuracy for PPP/INS integrated positioning can be degraded by the gross error in GPS observation. The improved robust Kalman filter with the IGG principle was employed in PPP/INS tightly coupled positioning to remove the harmful effects from gross error of GPS pseudorange observation. Compared with the standard Kalman filter, the improved robust Kalman filter accuracy regarding the east, north and down components can be improved by 33%, 40% and 47%, respectively. The improved robust Kalman filter is very effective in identifying a simulated gross error added to GPS pseudo-range observation, which proves its good performance.

Acknowledgements

The work was partially sponsored by China's Post-doctoral Science Fund (grant number: 2015M580490) and partially sponsored by Natural Science Foundation of Jiangsu Province (grant number: BK20160247). The authors would like to thank Dr. Xiaolin Meng and all experienced members in the University of Nottingham for their help in collecting and processing the field test data.

Brought to you by | Politechnika Swietokrzyska - Kielce University of Technology
Authenticated
Download Date | 7/26/17 1:11 PM

References

[1] Chu, H.J., Tsai, G.J., Chiang, K.W., Duong, T.T. (2013). GPS/MEMS INS data fusion and map matching in urban areas. *Sensors*, 13(9), 11280–11288.

[2] Nassar, S. (2003). *Improving the Inertial Navigation System (INS) Error Model for INS and INS/DGPS Applications*. Ph.D. Thesis. The University of Calgary.

[3] Kouba, J., Héroux, P. (2001). Precise point positioning using IGS orbit and clock products. *GPS Solut.*, 5(2), 12–28.

[4] Du, S., Gao, Y. (2012). Inertial aided cycle slip detection and identification for integrated PPP GPS and INS. *Sensors*, 12(11), 14344–14362.

[5] Ali, J., Ushaq, M. (2009). A consistent and robust Kalman filter design for in-motion alignment of inertial navigation system. *Measurement*, 42(4), 577–582.

[6] Gao, S., Zhong, Y., Li, W. (2011). Robust adaptive filtering method for SINS/SAR integrated navigation system. *Aerosp. Sci. Technol.*, 15(6), 425–430.

[7] Huang, G., Zhang, Q. (2012). Real-time estimation of satellite clock offset using adaptively robust Kalman filter with classified adaptive factors. *GPS Solut.*, 16(4), 531–539.

[8] Guo, F., Zhang, X. (2014). Adaptive robust Kalman filtering for precise point positioning. *Meas. Sci. Technol.*, 25(10), 1–8.

[9] Chang, G. (2014). Robust Kalman filtering based on Mahalanobis distance as outlier judging criterion. *J. Geod.*, 88(4), 391–401.

[10] Du, S. (2010). *Integration of precise point positioning and low cost MEMS IMU*. Ph.D. Thesis. The University of Calgary.

[11] Abdel-salam, M.A. (2005). *Precise point positioning using un-differenced code and carrier phase observations*. Ph.D. Thesis. The University of Calgary.

[12] Titterton, D. (2004). *Strapdown inertial navigation technology*. 2nd ed. MIT Lincoln Laboratory.

[13] Han, S., Wang, J. (2012). Integrated GPS/INS navigation system with dual-rate Kalman Filter. *GPS Solut.*, 16(3), 389–404.

[14] Li, Z., Wang, J., Li, B., Gao, J., Tan, X. (2014). GPS/INS/Odometer integrated system using fuzzy neural network for land vehicle navigation applications. *J. Navigation*, 67(6), 967–983.

[15] Zhang, Y., Gao, Y. (2008). Integration of INS and un-differenced GPS measurements for precise position and attitude determination. *J. Navigation*, 61(1), 87–97.

[16] Nassar, S., El-Sheimy, N. (2006). A combined algorithm of improving INS error modeling and sensor measurements for accurate INS/GPS navigation. *GPS Solut.*, 10(1), 29–39.

[17] Chang, G. (2014). Kalman filter with both adaptivity and robustness. *J. Process Contr.*, 24(3), 81–87.

[18] Yang, Y. (1994). Robust estimation for dependent observations. *Manuscripta Geodaetica*, 19(1), 10–17.

Brought to you by | Politechnika Swietokrzyska - Kielce University of Technology
Authenticated
Download Date | 7/26/17 1:11 PM